Angle-resolved and resonant photoemission spectroscopy on heavy-fermion superconductors Ce_2CoIn_8 and Ce_2RhIn_8

S. Raj,* Y. Iida, S. Souma, T. Sato, and T. Takahashi
Department of Physics, Tohoku University, Sendai 980-8578, Japan

H. Ding
Department of Physics, Boston College, Chestnut Hill, Massachusetts 02467, USA

S. Ohara, T. Hayakawa, G. F. Chen, and I. Sakamoto
Department of Engineering Physics, Electronics and Mechanics, Nagoya Institute of Technology, Nagoya 466-8555, Japan

H. Harima
Department of Physics, Kobe University, Kobe 657-8501, Japan
(Received 12 November 2004; revised manuscript received 22 February 2005; published 30 June 2005)

We have carried out high-resolution angle-resolved and resonant photoemission spectroscopy (RPES) on heavy-fermion superconductors Ce_2CoIn_8 and Ce_2RhIn_8 to study the electronic band structure and the nature of the Ce $4f$ electrons. We have experimentally determined the valence-band structure and compared them with the full-potential linear augmented plane-wave band calculations. We found that both compounds have quasi-two-dimensional cylindrical Fermi surfaces centered at the $M(A)$ point in the Brillouin zone, which may be an essential parameter for the development of the superconductivity. Comparison with the band calculations based on the itinerant and localized models suggests that the Ce $4f$ electrons are essentially localized in both compounds at a measured temperature of 40 K. RPES results have confirmed the localized character of the Ce $4f$ electrons in both compounds, with a relatively stronger localized nature in Ce_2RhIn_8 than in Ce_2CoIn_8. This difference in the strength of localized character well explains the difference in the magnetic properties between the two compounds.

DOI: 10.1103/PhysRevB.71.224516 PACS number(s): 79.60.−i, 71.27.+a, 71.18.+y

I. INTRODUCTION

The development of superconductivity in heavy-fermion compounds has attracted much attention in condensed matter physics. The cause of superconductivity in heavy-fermion compounds is thought to be not the same as that of conventional BCS superconductors. In conventional superconductors, the electron-electron bound state mediated by lattice vibration, which ultimately forms the Cooper pair,[1] is responsible for the cause of superconductivity, while in heavy-fermion systems the electron-electron bound state may be magnetically mediated,[2] leading to superconductivity with a very low critical temperature T_c. Although there is no established mechanism which fully explains all the characteristic behavior of this type of superconductivity, the spin fluctuation at very low temperature is regarded as one of the potential causes in heavy-fermion superconductivity. It has been shown that both the ferromagnetic (i.e., spin triplet) and antiferromagnetic (i.e., spin singlet) states in different systems lead to magnetically mediated superconductivity.[2,3]

Recently, Ce-based compounds with a broader family of $Ce_n T In_{(3n+2)}$, where T is a transition metal (Co or Rh), were found to be heavy-fermion compounds and show superconductivity at very low temperatures. They crystallize in the tetragonal $Ho_n CoIn_{(3n+2)}$-type crystal structure ($P4/mmm$). The structure of $Ce_n T In_{(3n+2)}$ has n layers of $CeIn_3$, stacked sequentially with intervening one layer of $T In_2$ along the c axis.[4,5] The crystal structure of the parent compound $CeIn_3$ ($n=\infty$) is shown in Fig. 1(a). The $n=1$ compound has $CeIn_3$ and $T In_2$ alternating layers as shown in Fig. 1(b). These compounds are well known as Ce-115 compounds. The cobalt compound $CeCoIn_5$ is a heavy-fermion superconductor

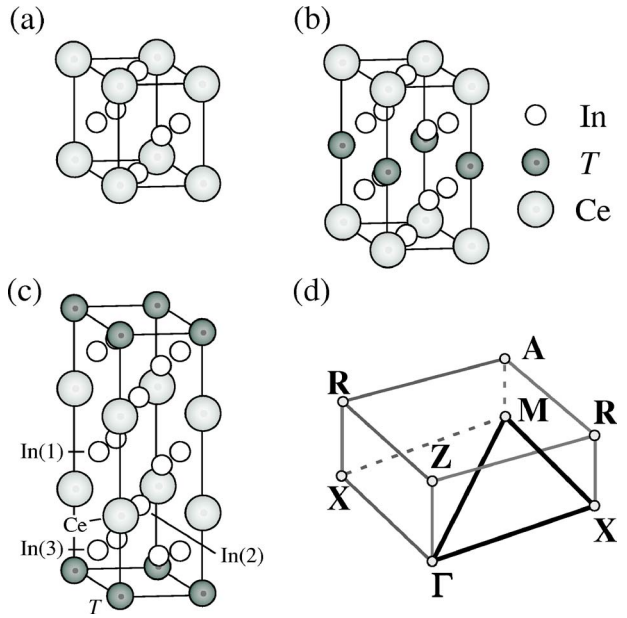

FIG. 1. Crystal structures of (a) $CeIn_3$, (b) $Ce T In_5$, and (c) $Ce_2 T In_8$, where T=Co or Rh. (d) Brillouin zone of $Ce_2 T In_8$.

with a transition temperature of T_c=2.3 K (Ref. 6) at ambient pressure. The electronic specific heat coefficient γ is about 300 mJ/(K^2 mol). On the other hand, $CeRhIn_5$ is an antiferromagnet with the Nèel temperature of T_N=3.8 K (Ref. 7) and the γ value is about 420 mJ/(K^2 mol). $CeRhIn_5$ undergoes a superconducting transition at T_c=2.1 K under pressure of 1.6 GPa. For n=2 system, the number of $CeIn_3$ layer increases with two $CeIn_3$ layers being stacked in between $T\,In_2$ layers as shown in Fig. 1(c). These compounds are known as Ce-218 compounds. The cobalt compound Ce_2CoIn_8 is a paramagnet and undergoes the superconducting transition at T_c=0.4 K (Ref. 8) at ambient pressure with the γ value more than 500 mJ/(K^2 mol). In contrast, Ce_2RhIn_8 is an antiferromagnet with T_N=2.8 K and becomes superconductive at T_c=1.1 K (Ref. 9) under pressure of 1.63 GPa. The γ value is about 370 mJ/(K^2 mol). The electronic specific heat coefficient γ is very large in these Ce-218 compounds at low temperature, showing the quasiparticle nature characteristic of heavy fermions. In addition, de Haas–van Alphen (dHvA) experiments have also demonstrated the presence of heavy electron effective mass at low temperature in both these Ce-115 and Ce-218 compounds.[10–16] The effective mass of the conduction electron increases due to the presence of magnetic Ce ions in these heavy-fermion compounds.

There are several reports available for Ce-115 compounds on the Fermi surface (FS) topology[10–15,17] and the band structure calculation.[18–20] However, a limited number of works in the literature are available for Ce-218 compounds on their physical properties. Ueda *et al.*[16] performed dHvA experiment together with some physical-properties measurements for both Ce_2RhIn_8 and La_2RhIn_8 and reported that the Ce 4*f* electrons are localized in Ce_2RhIn_8. In contrast to the dHvA experiment, angle-resolved photoemission spectroscopy (ARPES) has a capability to directly identify the character of the FS (electron or hole like) as well as the exact location in the Brillouin zone (BZ). In Ce_2CoIn_8 and Ce_2RhIn_8, only a single *f* electron of the Ce atom is expected to participate in both the magnetism and superconductivity through its hybridization with conduction electrons. So understanding of the magnetic properties, the electronic structures, and the character of Ce 4*f* electrons is essential to elucidate the mechanism of the superconductivity in these compounds.

In this paper, we report results of ARPES and resonant photoemission (RPES) studies on Ce_2CoIn_8 and Ce_2RhIn_8. We have succeeded in experimentally determining the valence-band structure as well as the FS. The FS shows a two-dimensional cylindrical shape centered at the $M(A)$ point in the BZ [Fig. 1(d)], reflecting the layered structure. The Ce 4*d*-4*f* RPES results clearly identify the nature of Ce 4*f* electrons in these compounds, showing that the Ce 4*f* electrons are essentially localized in both compounds at the measured temperature, 40 K, with a relatively stronger localized nature in the rhodium compound than in the cobalt counterpart.

II. EXPERIMENTS

Single crystals of Ce_2CoIn_8 and Ce_2RhIn_8 were grown with the indium flux method. The details of sample preparation have been described elsewhere.[8,21] ARPES measurements were performed using a GAMMADATA SCIENTA SES 2002 spectrometer with 22-eV photons at the undulator 4m-NIM beamline at the Synchrotron Radiation Center in Wisconsin. In ARPES measurements, we rotated the sample with respect to the incident light and the analyzer. The angle between the incident light and the analyzer is fixed at 45°. The polarization of incident light is therefore always in the electron emission plane for the measurements of the $\Gamma(Z)$-$X(R)$ and $\Gamma(Z)$-$M(A)$ directions, but not in the same plane for the $M(A)$-$X(R)$ direction. RPES measurements were carried out with 122-eV and 114-eV photons at the undulator PGM beamline in the same facility. The energy and angular (momentum) resolutions were set at 20–35 meV and 0.2° (0.01 $Å^{-1}$), respectively. The measurements were performed at 40 K in a vacuum of 5×10^{-11} Torr. A clean surface of sample for photoemission measurements was obtained by *in situ* cleaving of the crystal along the (001) plane. After each set of measurement we checked the degradation of sample surface and found no degradation to the surface. The Fermi level (E_F) of sample was referred to that of a gold film evaporated on the sample substrate.

III. BAND CALCULATIONS

We have carried out the full-potential linear augmented plane-wave (FLAPW) band structure calculation by using the program code KANSAI-03 (Ref. 22) for Ce_2CoIn_8 and Ce_2RhIn_8, where we assumed the Ce 4*f* electrons being itinerant. We have also calculated the band structure for La_2CoIn_8 and La_2RhIn_8, which are regarded as the reference compounds of Ce_2CoIn_8 and Ce_2RhIn_8 with localized Ce 4*f* electrons, respectively. The band structure calculations for Ce_2RhIn_8 and La_2RhIn_8 have been carried out by using the lattice parameter of Ce_2RhIn_8 with a=4.663 25 Å and c =12.2443 Å. The atomic positions (x,y,z) of Ce, Rh, In(1), In(2), and In(3) in the unit cell are (0, 0, 0.308 39), (0, 0, 0), (0, 0.5, 0.5), (0.5, 0.5, 0.306 95), and (0, 0.5, 0.117 93), respectively[23] [see Fig. 1(c)]. We have taken 63 k points for the potential convergence and 330 k points for the final band structure and all the sampling points are uniformly distributed in the irreducible 1/16th of the Brillouin zone (IBZ). The details of band calculations for Ce_2RhIn_8 and La_2RhIn_8 have been described elsewhere.[16] The calculations for Ce_2CoIn_8 and La_2CoIn_8 have been performed by using the same method as for Ce_2RhIn_8 and La_2RhIn_8, except using the 220 k sampling points in the Brillouin zone for both the potential convergence and the final band structure calculations. In the band calculations for both Ce_2CoIn_8 and La_2CoIn_8 we have used the lattice parameter of Ce_2CoIn_8 with a=4.646 Å and c=12.251 Å. The atomic positions of Ce, Co, In(1), In(2), and In(3) in the unit cell are (0, 0, 0.3105), (0, 0, 0), (0, 0.5, 0.5), (0.5, 0.5, 0.2962), and (0, 0.5, 0.1199), respectively.[23] From the calculated partial density of states (DOS) (not shown), it is clear that the near-E_F region is mainly from the In 5*p* states and the higher-binding-energy region is dominated by the *d* states of Co or Rh in both (itinerant and localized) calculations. In the itinerant model

the Ce $4f$ partial DOS lies very close to E_F by mixing with the In $5p$ states, where it is well below E_F in the localized model.

IV. RESULTS AND DISCUSSION

A. Valence-band region

Figure 2(a) shows valence-band ARPES spectra of Ce_2CoIn_8 measured at 40 K with 22-eV photons along the $\Gamma(Z)$-$X(R)$, $\Gamma(Z)$-$M(A)$, and $X(R)$-$M(A)$ high-symmetry lines in the BZ. The spectra show several dispersive bands, in particular in the energy range within 1 eV from E_F. In the $\Gamma(Z)$-$X(R)$ direction, we find a nondispersive small peak near E_F (marked as A_1) with a relatively stronger intensity between the $\Gamma(Z)$ and $X(R)$ points. We also find another peak at 0.3 eV (marked as B_1) at the $\Gamma(Z)$ point, which disperses toward the high binding energy on going to the $X(R)$ point. Two peaks located at 0.7 eV and 1 eV (marked as C_1 and D_1), respectively, at the $\Gamma(Z)$ point show an upward dispersion, and one of them (C_1) looks to merge with band B_1 near the $X(R)$ point. A weak nondispersive band observed around 2 eV is gradually vanished as it moves to the $X(R)$ point. Similar to the $\Gamma(Z)$-$X(R)$ direction, we also find several dispersive peaks near E_F in the $\Gamma(Z)$-$M(A)$ direction. We find in Fig. 2(a) that a dispersive band (band A_2) enters from the unoccupied states into the occupied states at a point a little away from the $\Gamma(Z)$ point, forming a holelike FS centered at the $\Gamma(Z)$ point. Band A_2 gradually disperses toward the high binding energy and merges with the lower-lying band (band B_2) at the middle on the way to the $M(A)$ point. We observe a slightly dispersive band (band C_2) at 0.7 eV similar to band C_1 in the $\Gamma(Z)$-$X(R)$ direction. Band D_2 at 1 eV shows a steep upward dispersion around the $\Gamma(Z)$ point and then slowly disperses toward the high binding energy. In contrast to band E_1 in the $\Gamma(Z)$-$X(R)$ direction, band E_2 exhibits a steep downward dispersion around the $\Gamma(Z)$ point. Finally in the $X(R)$-$M(A)$ direction, two dispersive bands (A_3 and B_3) cross E_F midway between the $X(R)$ and $M(A)$ points. A nearly nondispersive band (C_3) is seen at 0.5 eV, and a very weak structure (D_3) with small energy dispersion is observed at 1–1.5 eV.

In order to see more clearly the band dispersion, we have mapped out the band structure and show the results in Figs. 2(b) and 2(c). The experimental band structure has been obtained by taking the second derivative of ARPES spectra and plotting the intensity by gradual shading as a function of the wave vector and the binding energy. The dark areas correspond to the experimental bands. The experimental band structure is compared with the theoretical band calculations of Ce_2CoIn_8 with itinerant Ce $4f$ electrons and La_2CoIn_8 which is regarded as a reference to Ce_2CoIn_8 with localized Ce $4f$ electrons in Figs. 2(b) and 2(c), respectively. In both Figs. 2(b) and 2(c) we clearly see many dispersive experimental bands in all the high-symmetry lines. By comparing with the calculation, we assign the experimental bands located around 0.5 eV to the Co $3d$ states while the other bands located at higher binding energy are due to the hybridization between the Co $3d$ and the In $5s$ and $5p$ states. It is noted that the Ce $4f$ band (level) is hard to directly observe because the Ce $4f$ photoionization cross section is very low at the present 22 eV incident photon energy.[24] We clearly see two bands (A_3 and B_3) cross E_F near the $X(R)$ point in the $M(A)$-$X(R)$ direction, similar to the Ce-115 compounds.[25] We find a fairly good qualitative agreement between the experiment and both the calculations near E_F around the $M(A)$

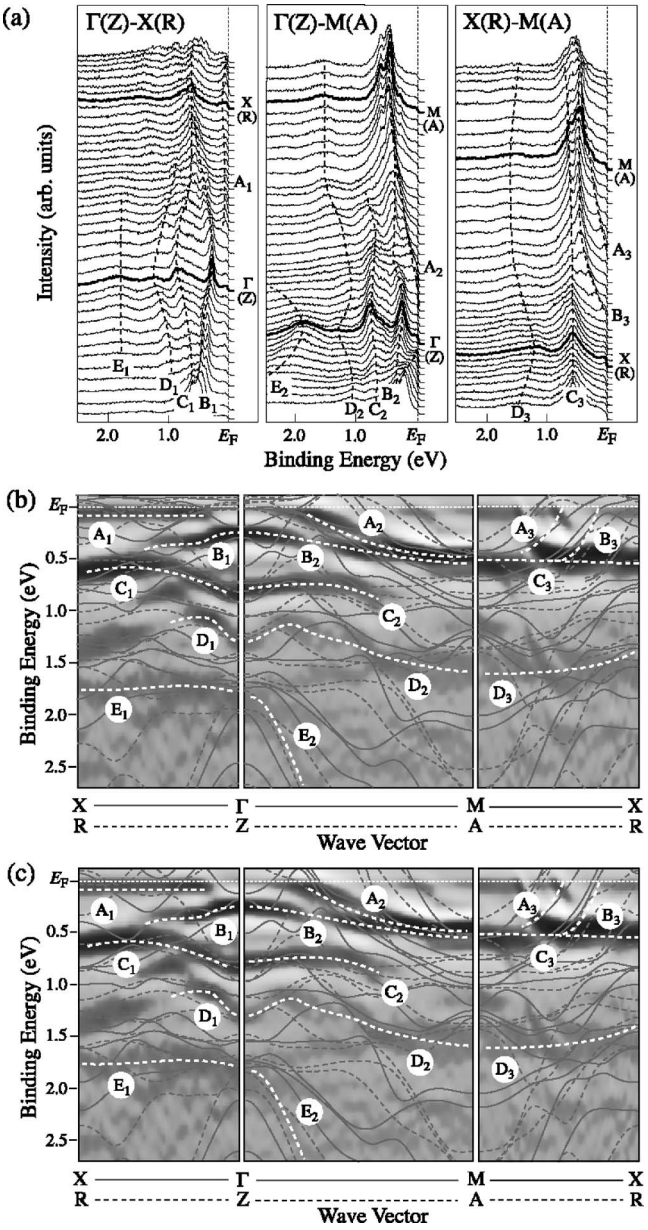

FIG. 2. (a) Valence-band ARPES spectra of Ce_2CoIn_8 measured at 40 K with 22-eV photons along the $\Gamma(Z)$-$X(R)$, $\Gamma(Z)$-$M(A)$, and $X(R)$-$M(A)$ high-symmetry lines. (b) Band structure of Ce_2CoIn_8 obtained from the second derivative of ARPES spectra. Dark areas correspond to the experimental bands and white dashed lines are guide to the experimental bands. Theoretical band structure of Ce_2CoIn_8 calculated along the high-symmetry lines with the FLAPW method is also shown by thin solid and dashed lines for comparison. (c) Same as (b) but with comparison to the band calculation of La_2CoIn_8, which is a reference compound to Ce_2CoIn_8 with localized Ce $4f$ electrons.

point as well as in the high-binding-energy region, while there are obvious discrepancies near E_F around the $\Gamma(Z)$ point.

In ARPES experiment the wave vector perpendicular to the surface, $k_\perp$, is rather difficult to control. However, it is well known that the high-symmetry lines in the Brillouin zone are likely to appear as a prominent well-resolved structure in the ARPES spectrum because of the relatively large DOS on the high-symmetry lines and the $k_\perp$ broadening due to the short escape depth.[26] Hence it is expected that the present ARPES data reflect the electronic structure mainly of two sets of high-symmetry lines, $\Gamma X(ZR)$ and $\Gamma M(ZA)$, enabling the comparison of the experimental band structure obtained by ARPES with the band calculations on the high-symmetry lines. It is also remarked here that the energy dispersion of all experimental bands matches quite well the bulk crystal periodicity, showing that the observed energy bands are mainly of bulk origin.

Figure 3 shows the valence-band ARPES spectra of Ce_2RhIn_8, together with the experimental band structure derived from the ARPES experiment by using the same method as in the case of Ce_2CoIn_8. In Figs. 3(b) and 3(c), we compare the experimental band structure with the theoretical band calculations for Ce_2RhIn_8 and La_2RhIn_8, respectively. In the calculation for the former compound, the Ce $4f$ electrons are treated as itinerant and the latter compound is regarded as a reference to Ce_2RhIn_8 with localized Ce $4f$ electrons. It is expected that the valence band will consist of mainly the Rh $4d$ and the In $5s$ and $5p$ states with contributions from the Ce $4f$ states near E_F. Along the $\Gamma(Z)$-$X(R)$ direction, two experimental bands (A_1 and B_1) cross E_F near the $\Gamma(Z)$ point, while there is no signature of band crossing near the $X(R)$ point. A band (marked as E_1) with 0.5 eV binding energy around the $\Gamma(Z)$ point is assigned to the Rh $4d$ states. In the high-binding-energy region, there are at least four dispersive bands (F_1, G_1, H_1, and I_1), and the former three bands have a stronger intensity around the $X(R)$ point while the last one is prominent around the $\Gamma(Z)$ point. In the $\Gamma(Z)$-$M(A)$ direction, four bands (A_2, B_2, C_2, and D_2) look to cross E_F, and three of them (B_2, C_2, and D_2) form electronlike FS's centered at the $M(A)$ point while band A_2 forms a holelike FS at the $\Gamma(Z)$ point. In the $X(R)$-$M(A)$ direction, we observe several dispersive band which show a smooth connection to the bands in both $\Gamma(Z)$-$X(R)$ and $\Gamma(Z)$-$M(A)$ directions. In the whole experimental band structure, we clearly find one holelike FS at the $\Gamma(Z)$ point formed by band A (A_1, A_2) and three electronlike FS's centered at the $M(A)$ point originating in bands B, C, and D. Similar holelike and electronlike FS's centered at the $\Gamma(Z)$ and $M(A)$ points have been also observed in Ce-115 compounds.[12,17] As seen in Figs. 3(b) and 3(c), the theoretical band calculations for both itinerant (for Ce_2RhIn_8) and localized (for La_2RhIn_8) models reproduce fairly well the experimentally obtained band structure in the high-binding-energy region (from 1 to 4 eV). In contrast, in the near-E_F region, we find several discrepancies between the experiment and calculations. For example, an experimentally observed small electron pocket centered at the $M(A)$ point is not reproduced either in the two band calculations. The itinerant band calculation predicts several slowly dispersive bands near E_F due to the mixture with the Ce $4f$ states, while the ARPES results do not show such a flatband near E_F, but exhibit some highly dispersive straight bands across E_F. Thus, at this stage, it is hard to finally conclude the character (itinerant or localized) of Ce $4f$ electrons in Ce_2RhIn_8 only from the whole valence band structure and it is necessary to study the detail of the electronic structure near E_F.

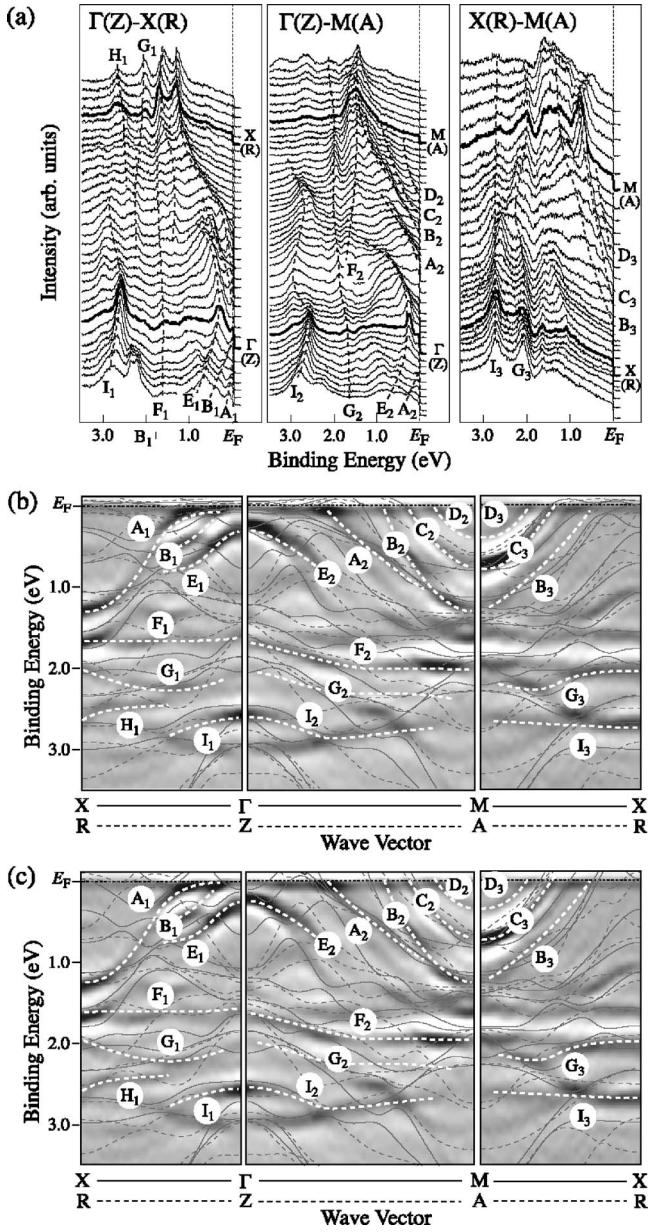

FIG. 3. (a) Valence-band ARPES spectra of Ce_2RhIn_8 measured at 40 K with 22-eV photons along the three high-symmetry lines. (b) Band structure of Ce_2RhIn_8 obtained from the second derivative of ARPES spectra. Dark areas correspond to the experimental bands and white dashed lines are guide to the experimental bands. Theoretical band structure of Ce_2RhIn_8 with itinerant Ce $4f$ electrons is shown by thin solid and dashed lines for comparison. (c) Same as (b) but with comparison to the band calculation of La_2RhIn_8.

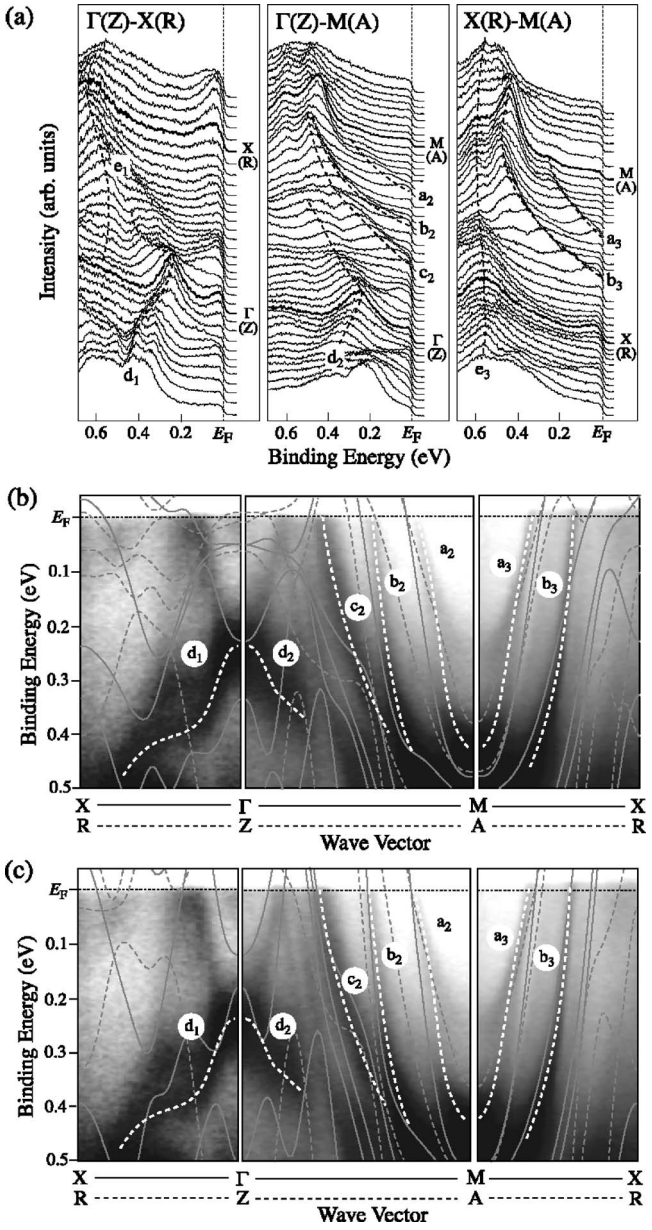

FIG. 4. (a) ARPES spectra near E_F of Ce_2CoIn_8 measured with 22-eV photons at 40 K along the three high-symmetry lines. (b) Experimental band structure of Ce_2CoIn_8. Dark areas correspond to the bands and white dashed lines are guide to them. The theoretical band structure calculated based on the itinerant model is also shown by thin solid and dashed lines for comparison. (c) Same as (b) but with comparison to the band calculation of La_2CoIn_8.

B. Near-E_F region

In order to study the electronic structure near E_F in more detail we have carried out high-resolution ARPES measurements near E_F with a smaller energy interval and a higher signal-to-noise ratio. Figure 4(a) shows the high-resolution ARPES spectra near E_F of Ce_2CoIn_8 measured at 40 K with 22-eV photons along the high-symmetry directions in the BZ. Figures 4(b) and 4(c) show the plot of ARPES intensity as a function of the wave vector and the binding energy, showing the experimental band structure. The reason why we did not use the second derivative method to map out the band structure near E_F is to avoid an artifact from the Fermi-edge cutoff, which may produce a flat ghost band just at E_F due to the sharp drop-off of the spectral intensity at E_F. We find in Fig. 4 much more detailed dispersive features of bands near E_F as compared with Fig. 2. We also compare the band calculations of Ce_2CoIn_8 with itinerant Ce $4f$ electrons and La_2CoIn_8 which is regarded as a reference to Ce_2CoIn_8 with localized Ce $4f$ electrons in Figs. 4(b) and 4(c), respectively. We find three electronlike FS's (bands a_2, b_2, c_2) centered at the $M(A)$ point in the experiment, in qualitatively good agreement with both the band calculations, although theoretical bands close to each other are not well resolved in the experiment. In contrast, the discrepancy between the experiment and in both the calculations is apparent near the $\Gamma(Z)$ point. For example, although the itinerant band calculation predicts the band-bending behavior near E_F ($E_F-0.1$ eV) due to the strong mixture of the In $5p$ states and the Ce $4f$ level around the $\Gamma(Z)$ point, we have not observed such behavior of bands in the corresponding energy and momentum region. Thus the itinerant model does not satisfactorily describe the electronic structure near E_F of Ce_2CoIn_8, suggesting the localized nature of the Ce $4f$ electrons in this compound at the present measured temperature, 40 K. In Figs. 4(b) and 4(c), the intense band c_2 crosses the Fermi level and corresponds to a bundle of dispersive bands, whereas in Fig. 4(b) the calculated bands bend at E_F. In Fig. 4(c), the band calculation based on localized model shows the straight features across E_F and agrees well with the experimental intense band c_2. We find an electronlike pocket at the $\Gamma(Z)$ point in the experiment, which may correspond to a small electron pocket in the localized band calculation [see Fig. 4(c)]. Since Ce_2CoIn_8 does not show any magnetic transition in all temperature ranges similar to $CeCoIn_5$, it is believed that the ground state at very low temperature may be different from the present high-temperature state. The presence of nondispersive structure at E_F around the $X(R)$ point in Fig. 4(a) may be an indication of the Ce $4f$ hybridized states.

We have also measured ARPES spectra near E_F for Ce_2RhIn_8 with high accuracies and show the results in Fig. 5. In Figs. 5(b) and 5(c), we compare the experimentally determined band structure with the band calculations for Ce_2RhIn_8 with itinerant Ce $4f$ electrons and La_2RhIn_8, respectively. As described above, the latter compound is regarded as a reference to Ce_2RhIn_8 with localized Ce $4f$ electrons. In the experiment, we have observed three electronlike FS's (bands d, e, and f) centered at the $M(A)$ point along with one holelike FS (band g) at the $\Gamma(Z)$ point in qualitatively good agreement with the calculations, although the position of the E_F crossing shows a deviation, in particular for the smallest FS, between the experiment and the calculation. It is remarked here that bands d, e, and f are very sharp in contrast to the broad feature of band g. This suggests that the FS's constructed by bands d, e, and f are highly two dimensional along the c axis, reflecting the layered crystal structure. Band g shows a very steep dispersion across E_F near the $\Gamma(Z)$ point. This experimental band shows a good correspondence to a bundle of a few highly dispersive bands located in the same energy and momentum region in the

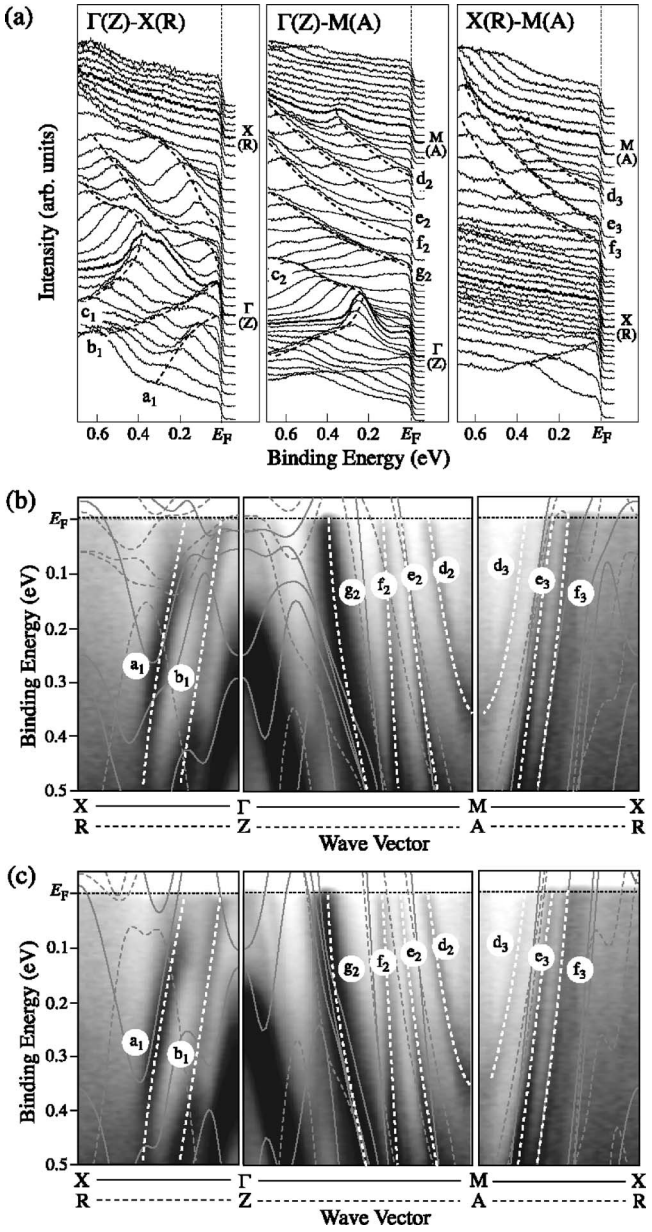

FIG. 5. (a) ARPES spectra near E_F of Ce_2RhIn_8 measured with 22-eV photons at 40 K along the three high-symmetry lines. (b) Experimental band structure of Ce_2RhIn_8. Dark areas correspond to the bands and white dashed lines are guide to them. The theoretical band structure of Ce_2RhIn_8 with itinerant Ce $4f$ electrons is shown by thin solid and dashed lines for comparison. (c) Same as (b) but with comparison to the band calculation of La_2RhIn_8.

band calculation of La_2RhIn_8 [see Fig. 5(c)]. In contrast, in the band calculation of Ce_2RhIn_8 based on the itinerant model, we do not find such straight bands across E_F. The absence of straight bands near E_F in the calculation is due to the presence of itinerant Ce $4f$ electrons near E_F, which strongly hybridize with the In $5p$–Rh $4d$ bands and consequently bend otherwise straight In $5p$–Rh $4d$ bands near E_F. This characteristic difference in the band structure near E_F between the two band calculations is essential to distinguish the nature of the Ce $4f$ electrons in Ce_2RhIn_8. In light of the straight feature of the In $5p$–Rh $4d$ band across E_F, it is concluded that the Ce $4f$ electrons in Ce_2RhIn_8 have a strong localized nature as in $CeRhIn_5$ compound.[16]

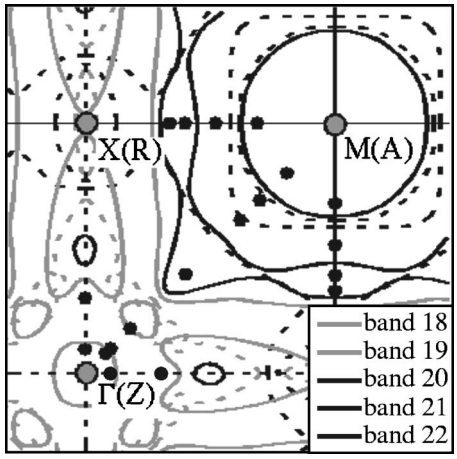

FIG. 6. Calculated Fermi surfaces of La_2RhIn_8 on the Γ*XMX* (solid lines) and *ZRAR* (dashed lines) planes. Gray and black lines correspond to holelike and electronlike FS's, respectively. Fermi vectors (k_F) determined by ARPES experiments are plotted with solid circles for comparison.

C. Fermi surface topology

In order to study the FS topology of Ce_2RhIn_8, we have determined the k_F positions along all the high-symmetry lines by following the experimental band dispersions near E_F, and show the results in Fig. 6, where the theoretical FS's calculated based on the localized model for the two high-symmetry planes (Γ*XMX* and *ZRAR* planes) in the BZ are also shown for comparison. We find that the FS topology is essentially similar for Ce_2CoIn_8 and Ce_2RhIn_8. In the $\Gamma(Z)$-$M(A)$ direction, we have found six k_F points at 0.09, 0.18, 0.40, 0.63, 0.71, and 0.81 Γ*M* from the Γ point. The former two k_F points correspond to the complicated holelike FS's around the $\Gamma(Z)$ point while the latter four k_F points belong to the electronlike FS's centered at the $M(A)$ point. We find a fairly good agreement in the k_F position between the experiment and calculation except for the smallest electronlike FS at the $M(A)$ point. In Ce_2CoIn_8 we observe clearly an electronlike pocket at the $\Gamma(Z)$ point [Figs. 4(b) and 4(c)], which agrees well with the localized theoretical prediction. In contrast, in Ce_2RhIn_8 [Figs. 5(b) and 5(c)] we observe a holelike pocket exactly at the same k_F position. This may be due to the strong intensity of the holelike band which covers the electronlike band in the band mapping. In contrast to the $\Gamma(Z)$-$M(A)$ direction, we have not observed any FS's centered at the $X(R)$ point contrary to the band calculation. This apparent disappearance of FS's around the $X(R)$ point in the experiment may be due to the strong three-dimensional character of the FS's as predicted from the band calculation. In contrast, the electronlike FS's centered at the $M(A)$ point are highly two dimensional, as evidenced by the very sharp feature of the corresponding bands in the experiment as shown in Fig. 5. This strong two-dimensional character of the FS's may be an essential condition for the development of super-

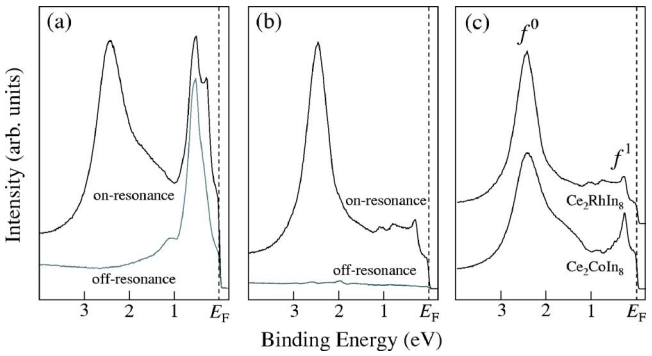

FIG. 7. (a) and (b) Ce 4*d*-4*f* on- and off-resonance PES spectra of Ce_2CoIn_8 and Ce_2RhIn_8, respectively. (c) Subtracted spectra for both compounds, obtained by subtracting the off-resonance spectrum from the corresponding on-resonance spectrum after normalizing the spectral intensity with the incident photon flux.

conductivity in these compounds. It is expected that the two-dimensional electronic structure gradually turns into the three-dimensional one as the number of $CeIn_3$ layer increases in the crystal structure (see Fig. 1). In these heavy-fermion compounds, the maximum value of T_c gradually decreases in accordance with the increase of the number of $CeIn_3$ layer, supporting the importance of two dimensionality for higher T_c. This is also supported from the dHvA experiments by Hall *et al.*,[10] who concluded that the increasingly two-dimensional electronic structure in $CeCoIn_5$ as compared to $CeIrIn_5$ has a direct correlation with the enhanced T_c, because $CeCoIn_5$ has a 5 times larger T_c than $CeIrIn_5$. Hence, the two-dimensional character of the electron pocket around the $M(A)$ point observed in both Ce_2CoIn_8 and Ce_2RhIn_8 is an essential condition for the development of superconductivity in this family of heavy-fermion compounds.

D. 4*d*-4*f* resonance spectra

In order to study the contribution from the Ce 4*f* states to the electronic structure near E_F as well as the nature of Ce 4*f* electrons, we have carried out the Ce 4*d*-4*f* RPES on Ce_2CoIn_8 and Ce_2RhIn_8 at a temperature 40 K. This resonance method utilizes the large resonant enhancement of the Ce 4*f* photoionization cross section near the Ce 4*d* core-level absorption threshold. Figures 7(a) and 7(b) show the on- and off-resonance spectra of Ce_2CoIn_8 and Ce_2RhIn_8 carried out at 122 and 114 eV incident photon energies, respectively. Figure 7(c) shows the comparison of angle-integrated valence-band spectra at the on-resonance condition after subtracting the corresponding off-resonance spectrum. This procedure has been used to derive the Ce 4*f* component in the spectra. The subtraction has been done after normalizing the spectral intensity with the incident photon flux. Both subtracted spectra clearly show the $f^1_{5/2}$ final-state peak located just at E_F together with its counter part, the $f^1_{7/2}$ final-state peak, at about 250 meV. The f^0 final-state peak is seen at 2.5 eV below E_F. These features are observed in various Ce-based compounds and well understood in terms of the single-impurity Anderson model (SIAM).[27] In the SIAM, the ground state is a linear combination of the f^0 and $f^1_{5/2}$ states due to the finite hybridization. Generally the f^0 peak is strong as compared to the f^1 peak when the Ce 4*f* electrons are localized. As seen in Figs. 7(a) and 7(b), the f^1 peak is heavily overlapped by the Co 3*d* peak at 0.5 eV in Ce_2CoIn_8 while such an interference is not seen in Ce_2RhIn_8. This is because the photoionization cross section of the Co 3*d* level is one order higher than that of the Rh 4*d* level at the Ce 4*d*-4*f* resonance photon energy (122 eV).[24] It is clear from Fig. 7(c) that the f^0 peak is much larger than the f^1 peak in both compounds, although the intensity ratio of the f^1 peak with respect to the f^0 peak is relatively smaller in Ce_2RhIn_8 than in Ce_2CoIn_8. This suggests that the Ce electrons in both compounds are essentially localized and those in Ce_2RhIn_8 have a stronger localized nature than those in Ce_2CoIn_8. This strong localized nature of Ce 4*f* electrons may be responsible for the antiferromagnetic transition at low temperature in Ce_2RhIn_8. This is consistent with the experimental fact that Ce_2CoIn_8, where the Ce 4*f* electrons are found to be relatively less localized than those in Ce_2RhIn_8, is paramagnetic in all temperature range.

V. CONCLUSION

We have carried out high-resolution angle-resolved and resonant photoemission spectroscopy on Ce_2CoIn_8 and Ce_2RhIn_8. We have experimentally determined the valence-band structure of both compounds and compared them with the band calculations where the Ce 4*f* electrons are treated as itinerant or localized. In both compounds, we found three quasi-two-dimensional cylindrical Fermi surfaces centered at the $M(A)$ point in the Brillouin zone, which may be responsible for the development of superconductivity. We found that the band calculation based on the localized model better describes the experimental band structure near E_F than the itinerant model. This suggests that the Ce 4*f* electrons in both compounds are essentially localized at the present measured temperature of 40 K. The RPES experimental results have confirmed this localized picture and, in addition, revealed that the Ce 4*f* electrons in Ce_2RhIn_8 have a relatively stronger localized nature than those in Ce_2CoIn_8. This difference in the localized character explains well the difference in the magnetic property between the two compounds.

ACKNOWLEDGMENTS

This work is supported by grants from the JSPS and MEXT of Japan.

*Electronic address: raj@arpes.phys.tohoku.ac.jp

[1] J. Bardeen, L. N. Cooper, and J. R. Schrieffer, Phys. Rev. **108**, 1175 (1957).
[2] N. D. Mathur, F. M. Grosche, S. R. Julian, I. R. Walker, D. M. Freye, R. K. W. Haselwimmer, and G. G. Lonzarich, Nature (London) **394**, 39 (1998).
[3] S. S. Saxena, P. Agarwal, K. Ahilan, F. M. Grosche, R. K. W. Haselwimmer, M. J. Steiner, E. Pugh, I. R. Walker, S. R. Julian, P. Monthoux, G. G. Lonzarich, A. Huxley, I. Sheikin, D. Braithwaite, and J. Flouquet, Nature (London) **406**, 587 (2000).
[4] E. G. Moshopoulou, Z. Fisk, J. L. Sarrao, and J. D. Thompson, J. Solid State Chem. **158**, 25 (2001).
[5] W. Bao, P. G. Pagliuso, J. L. Sarrao, J. D. Thompson, Z. Fisk, and J. W. Lynn, Phys. Rev. B **64**, 020401(R) (2001).
[6] C. Petrovic, P. G. Pagliuso, M. F. Hundley, R. Movshovich, J. L. Sarrao, J. D. Thompson, Z. Fisk, and P. Monthoux, J. Phys.: Condens. Matter **13**, L337 (2001).
[7] H. Hegger, C. Petrovic, E. G. Moshopoulou, M. F. Hundley, J. L. Sarrao, Z. Fisk, and J. D. Thompson, Phys. Rev. Lett. **84**, 4986 (2000).
[8] G. Chen, S. Ohara, M. Hedo, Y. Uwatoko, K. Saito, M. Sorai, and I. Sakamoto, J. Phys. Soc. Jpn. **71**, 2836 (2002).
[9] M. Nicklas, V. A. Sidorov, H. A. Borges, P. G. Pagliuso, C. Petrovic, Z. Fisk, J. L. Sarrao, and J. D. Thompson, Phys. Rev. B **67**, 020506(R) (2003).
[10] D. Hall, E. Palm, T. Murphy, S. Tozer, Z. Fisk, U. Alver, R. G. Goodrich, J. L. Sarrao, P. G. Pagliuso, and T. Ebihara, Phys. Rev. B **64**, 212508 (2001).
[11] R. Settai, H. Shishido, S. Ikeda, Y. Murakawa, M. Nakashima, D. Aoki, Y. Haga, H. Harima, and Y. Onuki, J. Phys.: Condens. Matter **13**, L627 (2001).
[12] D. Hall, E. Palm, T. Murphy, S. W. Tozer, C. Petrovic, E. Miller-Ricci, L. Peabody, Li Charis Quay Huei, U. Alver, R. G. Goodrich, J. L. Sarrao, P. G. Pagliuso, J. M. Wills, and Z. Fisk, Phys. Rev. B **64**, 064506 (2001).
[13] Y. Haga, Y. Inada, H. Harima, K. Oikawa, M. Murakawa, H. Nakawaki, Y. Tokiwa, D. Aoki, H. Shishido, S. Ikeda, N. Watanabe, and Y. Onuki, Phys. Rev. B **63**, 060503(R) (2001).
[14] H. Shishido, R. Settai, D. Aoki, S. Ikeda, H. Nakawaki, N. Nakamura, T. Iizuka, Y. Inada, K. Sugiyama, T. Takeuchi, K. Kindo, T. C. Kobayashi, Y. Haga, H. Harima, Y. Aoki, T. Namiki, H. Sato, and Y. Onuki, J. Phys. Soc. Jpn. **71**, 162 (2002).
[15] H. Shishido, R. Settai, S. Araki, T. Ueda, Y. Inada, T. C. Kobayashi, T. Muramatsu, Y. Haga, and Y. Onuki, Phys. Rev. B **66**, 214510 (2002).
[16] T. Ueda, H. Shishido, S. Hashimoto, T. Okubo, M. Yamada, Y. Inada, R. Settai, H. Harima, A. Galatanu, E. Yamamoto, N. Nakamura, K. Sugiyama, T. Takeuchi, K. Kindo, T. Namiki, Y. Aoki, H. Sato, and Y. Onuki, J. Phys. Soc. Jpn. **73**, 649 (2004).
[17] S. I. Fujimori, T. Okane, J. Okamoto, K. Mamiya, Y. Muramatsu, A. Fujimori, H. Harima, D. Aoki, S. Ikeda, H. Shishido, Y. Tokiwa, Y. Haga, and Y. Onuki, Phys. Rev. B **67**, 144507 (2003).
[18] J. Costa-Quintana and F. Lopez-Aguilar, Phys. Rev. B **67**, 132507 (2003).
[19] J. L. Wang, Z. Zeng, Q. Q. Zheng, and H. Q. Lin, J. Appl. Phys. **93**, 6891 (2003).
[20] T. Maehira, T. Hotta, K. Ueda, and A. Hasegawa, J. Phys. Soc. Jpn. **72**, 854 (2003).
[21] S. Ohara, Y. Shomi, and I. Sakamoto, J. Phys. Soc. Jpn. **71**, suppl. 258 (2002).
[22] H. Harima, computer code KANSAI-03, Kobe University, Kobe, Japan, 2003.
[23] P. Villans and L. D. Calvert, *Perarson's Handbook of Crystallographic Data for Intermetallic Phases*, 2nd ed. (ASM International, Ohio, 1991).
[24] J. Yeh and I. Lindau, At. Data Nucl. Data Tables **32**, 1 (1985).
[25] K. Kanai and S. Shin, RIKEN Rev. **46**, 10 (2002).
[26] F. J. Himpsel, Adv. Phys. **32**, 1 (1983).
[27] O. Gunnarsson and K. Schonhammer, Phys. Rev. B **28**, 4315 (1983).